Biology Direct

RESEARCH

Open Access

Utilizing liquid-liquid biopolymer regulators to predict the prognosis and drug sensitivity of hepatocellular carcinoma

Jianhao Li[1,2†], Han Chen[1,2†], Lang Bai[1,2*] and Hong Tang[1,2*]

Abstract

Background Liquid-liquid phase separation (LLPS) is essential for the formation of membraneless organelles and significantly influences cellular compartmentalization, chromatin remodeling, and gene regulation. Previous research has highlighted the critical function of liquid-liquid biopolymers in the development of hepatocellular carcinoma (HCC).

Methods This study conducted a comprehensive review of 3,685 liquid-liquid biopolymer regulators, leading to the development of a LLPS related Prognostic Risk Score (LPRS) for HCC through bootstrap-based univariate Cox, Random Survival Forest (RSF), and LASSO analyses. A prognostic nomogram for HCC patients was developed using LPRS and other clinicopathological factors. We utilized SurvSHAP to identify key genes within the LPRS influencing HCC prognosis. To validate our findings, we collected 49 HCC cases along with adjacent tissue samples and confirmed the correlation between DCAF13 expression and HCC progression through qRT-PCR analysis and in vitro experiments.

Results LPRS was established with 8 LLPS-related genes (TXN, CBX2, DCAF13, SLC2A1, KPNA2, FTCD, MAPT, and SAC3D1). Further research indicated that a high LPRS is closely associated with vascular invasion, histological grade (G3-G4), and TNM stage (III-IV) in HCC, concurrently establishing LPRS as an independent risk factor for prognosis. A nomogram that integrates LPRS with TNM staging and patient age markedly improves the predictive accuracy of survival outcomes for HCC patients. Our findings suggest that increased DCAF13 expression in HCC plays a crucial role in cancer progression and angiogenesis. Navitoclax has emerged as a promising treatment for HCC patients with high LPRS levels, offering a novel therapeutic direction by targeting LLPS.

Conclusion We have formulated a novel LPRS model that is capable of accurately predicting the clinical prognosis and drug sensitivity of HCC. DCAF13 might play a pivotal role in malignant progression mediated by LLPS.

Keywords Hepatocellular carcinoma, Liquid–liquid phase separation, DCAF13, Tumor microenvironment, Prognosis

†Jianhao Li and Han Chen contributed equally to this work.

*Correspondence:
Lang Bai
pangbailang@163.com
Hong Tang
tanghong6198@wchscu.cn

[1]Center of Infectious Diseases, West China Hospital of Sichuan University, Chengdu 610041, China
[2]Division of Infectious Diseases, State Key Laboratory of Biotherapy and Center of Infectious Diseases, West China Hospital of Sichuan University, Chengdu 610041, China

Introduction

Hepatocellular carcinoma (HCC) ranks third in global cancer mortality. Projections indicate that the incidence of HCC will exceed one million by 2025 [1–3]. Despite this alarming trend, early diagnosis of HCC occurs in fewer than 20% of cases, with more than half being diagnosed at advanced stages. Moreover, 70% of patients face recurrence within five years of initial treatment [4, 5]. Currently, the mainstays in treating HCC encompass surgical resection, percutaneous ethanol injection, and targeted therapy. While approximately 30% of patients initially exhibit favorable responses to sorafenib therapy, resistance typically emerges within six months [5]. In the past five years, immune checkpoint inhibitors have transformed HCC treatment, benefiting about 15–20% of patients [4, 6, 7]. Over the past decade, extensive research has been conducted on gene signatures for predicting the prognosis of HCC [8, 9]. However, these studies have predominantly focused on constructing models for overall patient prognosis, with limited relevance to the development of potential therapeutic targets and the selection of clinical treatment strategies [10]. In recent years, advancements in prognosis prediction for HCC have been significantly driven by studies focusing on specific biological processes, such as amino acid metabolism, RNA methylation, and cell death, which have also advanced the prediction of treatment responses [11–13]. Thus, developing HCC-specific prognostic biomarkers and identifying potential therapeutic targets based on distinct physiological and pathological processes is highly needed.

Liquid-liquid phase separation (LLPS) constitutes a biophysical process wherein biomolecules undergo rapid, reversible concentration to form liquid-phase condensates [14]. This process results in the formation of membrane-less organelles within cells, facilitating compartmentalization. These organelles and compartments play pivotal roles in diverse cellular functions, such as restructuring chromatin, overseeing gene transcription and translation, and more [15, 16]. The dynamism of LLPS involves active participation from scaffolds, regulators, and clients in this intricate molecular ballet. Scaffolds offer structural stability to biomolecular assemblies, while regulators guarantee their correct operation. Clients, which frequently include elements that bind particularly to scaffold elements, are found in condensates under certain conditions [14]. The LLPS status of key proteins, such as RNA-binding proteins and transcription factors, is known to influence their biological functions and downstream signaling regulation [17, 18]. For instance, the biomolecular condensate of the RNA-binding protein YTHDC1, generated through LLPS, is essential for safeguarding target mRNAs from degradation [19]. Recent studies have highlighted the connection between LLPS and various diseases, particularly neurodegenerative conditions like amyotrophic lateral sclerosis and Alzheimer's disease [20–24]. In HCC, early cancer cells convert absorbed glucose into glycogen for storage [25]. Excessive glycogen accumulation triggers LLPS, deactivating the tumor-suppressive Hippo signaling pathway and activating the oncogenic protein YAP, thereby initiating tumorigenesis [26]. Simultaneously, the autophagy substrate protein p62 modulates autophagy via LLPS, degrading damaged or non-membranous organelles and influencing HCC progression [27]. Therefore, we believe that exploring the role of LLPS in HCC research represents a valuable direction for enhancing our understanding of HCC pathogenesis, facilitating prognosis prediction, and guiding the personalized selection of therapeutic strategies.

In this study, we established a prognostic score for HCC and discovered potential treatment agents for high-LPRS patients. Concurrently, we screened and experimentally validated DCAF13 as a significant tumor promoter in HCC (Fig. 1). Initially, we developed an LLPS-Related prognostic risk score (LPRS) using differential analysis, the Random Survival Forest (RSF) method and LASSO regression. Extensive evaluations utilizing this marker, covering survival, clinical characteristics assessment, functional enrichment, tumor microenvironment analysis, and potential treatment agent screening, were conducted. We additionally combined the LPRS with other clinicopathological variables to create a prognostic nomogram for HCC patients. Using "SurvSHAP", we identified DCAF13 within the LPRS as a key prognostic gene, subsequently validating it through clinical tissue samples and in vitro cellular experiments. In conclusion, our research provides fresh perspectives on individualized prognosis prediction and the development of targeted therapies and drugs in HCC.

Materials and methods

Data source and preprocessing

Clinical data and gene expression information were gathered from public repositories, including The Cancer Genome Atlas (TCGA), International Cancer Genome Consortium (ICGC) databases and The National Omics Data Encyclopedia (NODE). To ensure comparability, all datasets underwent TPM normalization. Somatic mutations were scrutinized using the R package 'maftools'. For the HCC scRNA-seq dataset GSE149614, acquisition was done from the Gene Expression Omnibus (GEO) database. Cell subpopulation annotations were also obtained in this study [28]. Comprehensive details regarding specific cohorts and the number of clinical samples can be found in Table S1.

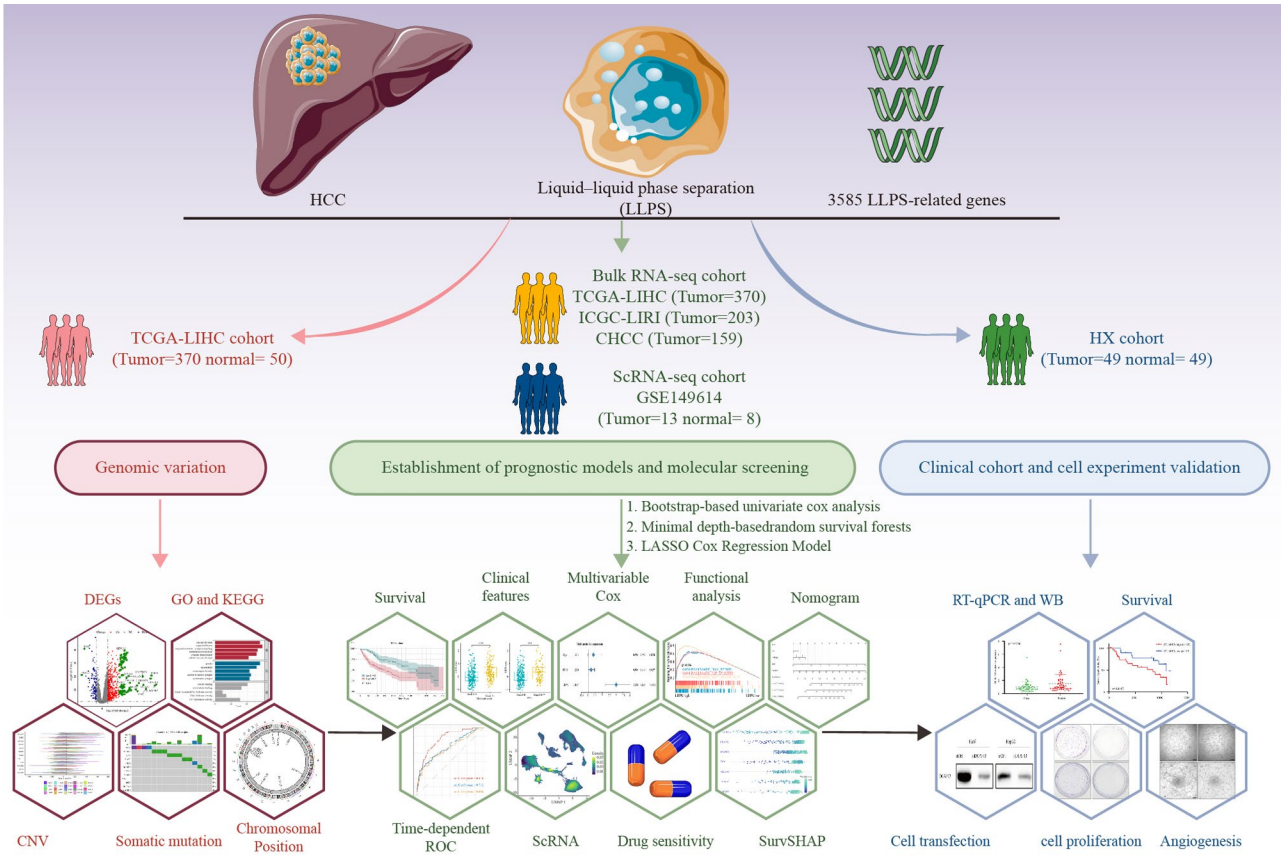

Fig. 1 Flowchart for comprehensive analysis of LLPS in HCC

Clinical samples

This study collected 49 HCC cases and adjacent tissue samples from patients who had liver resection at Western China Hospital of Sichuan University (2018–2019). The inclusion criteria were as follows: (1) patients who underwent curative resection for liver cancer, (2) postoperative pathological diagnosis confirmed HCC, and (3) no prior history of anticancer treatment. The exclusion criteria were: (1) patients with concurrent other malignancies and (2) patients who received antitumor therapy prior to surgery. Ethical guidelines were followed, informed consent was obtained, and the study was approved by the Ethics Committee of the hospital (2016–91), adhering to the Declaration of Helsinki.

Identification and validation of LPRS

Utilizing the data from the DrLLPS database, we analyzed gene expression data for 3,585 LLPS-related genes, including 85 scaffolds, 355 regulators, and 3,145 clients, from the TCGA cohort (Table S2) [29]. In the screening process, 652 differentially expressed genes (DEGs) were identified. DEGs associated with OS were then identified through univariate Cox regression analysis, yielding 330 significant DEGs. The data were subjected to 1000 rounds of bootstrapping, and 85 DEGs were consistently associated with prognosis in over 900 iterations. A Random Survival Forest (RSF) method, employing minimal depth (MD), was utilized to refine the selection of prognostically relevant genes, isolating 12 genes with the highest concordance index (C-index) values from 1,000 analyses. 12 genes were included in the LASSO Cox regression model to eliminate collinearity, and ultimately, 8 genes were selected for constructing the LPRS. The LPRS was computed with the following formula:

$$\mathrm{LPRS} = \sum_{i=1}^{n} \mathrm{Coefi}^{*}\mathrm{xi}$$

In this context, Coefi represents the coefficient, and xi denotes the mRNA expression value of eight regulators. This equation was utilized to compute the LPRS for each patient across both the training (TCGA) and validation (ICGC, CHCC) cohorts. The prognostic predictive efficacy of the LPRS in patients with HCC was assessed through the computation of time-dependent AUC.

Functional enrichment analysis

we employed the "clusterProfiler" package in R for the identification of potential biological pathways implicated by DEGs [30]. To further analyze the distinctive

biological functions between the high- and low- LPRS groups, we applied Gene Set Variation Analysis (GSVA) and Gene Set Enrichment Analysis (GSEA). The "h.all.v2022.1.Hs.symbols.gmt" database was employed for these analyses, facilitated by the R packages "GSVA" and "GSEABase."

Identification of potential therapeutic agents

In this study, patients were divided into LPRS-high and LPRS-low groups based on median LPRS scores. Human cancer cell line (CCL) data were sourced from the Cancer Cell Line Encyclopedia (CCLE) and the Dependency Map (DepMap) portal [31]. Drug sensitivity data were obtained from the PRISM Repurposing database and the Cancer Therapeutics Response Portal (CTRP), with a focus on determining drug sensitivity using the AUC. Our analysis aimed to find therapeutic agents showing higher sensitivity in LPRS-high groups by comparing AUC values and conducting Spearman correlation to identify drugs negatively correlated with LPRS scores. We compiled published clinical trial data and experimental evidence to ensure a comprehensive evaluation of candidate compounds [32]. This streamlined approach combines genomic and drug response data to identify potential treatments for HCC, highlighting the utility of integrated datasets in therapeutic discovery.

SurvSHAP

The SHAP (Shapley Additive exPlanations) framework, devised by Lundberg et al., revolutionizes the interpretability of "black box" machine learning (ML) models by quantifying individual feature contributions. This approach, facilitated by the "SurvSHAP" package, advances the field by offering detailed, time-dependent insights for survival regression deep learning models, thus enhancing the transparency and understanding of ML predictions [33, 34].

Cell culture and proliferation experiments

Huh7 and HepG2 HCC cell lines were obtained from Procell Life Science & Technology (Wuhan, China), and HUVECs from Cellcook (Guangzhou, China). HCC cells were cultured in DMEM with FBS at 37 °C and 5% CO2. HUVECs were cultured in EGM-2 BulletKit under similar conditions. Cell proliferation was measured using the CCK-8 assay. Briefly, 4000 cells were plated in 96-well plates, and viability was measured with a microplate reader. For the colony formation assay, 3000 cells were seeded and cultured for 10–14 days, then fixed, stained, and counted.

Cell transfection

DCAF13 siRNAs and the negative control (NC) were obtained from GenePharma (Shanghai, China). Transfections were done using Lipofectamine 3000 (Thermo Fisher, CA, USA) per the manufacturer's instructions. Transfection efficiency was verified 48 h later. The scrambled sequence was used as the NC siRNA.

Real-time quantitative PCR

Total RNA was extracted with TRIzol reagent (Invitrogen, USA) and converted to cDNA using the Prime Script™ RT reagent Kit (Takara, Japan). Quantitative PCR probes for DCAF13 were from Tsingke Biotechnology (Beijing, China). Gene expression was assessed in triplicate using the LightCycler96 (Roche, Switzerland) and C1000®®™ Thermal Cycler (Bio-Rad, USA), quantified by the $2^{-\Delta\Delta CT}$ method.

Western blotting

Cell lysates were prepared with RIPA buffer (Cell Signaling Technology). Western blotting used primary antibodies, including anti-DCAF13 (ab214424) and anti-HIF-1α (ab51608) from Abcam. Additional antibodies targeted HIF-1α, VEGF, NOTCH-1, β-catenin, c-Myc, and CCND1. Immune complexes were visualized with enhanced chemiluminescence reagents (4 A BIOTECH, Beijing, China).

Lumen formation assay

The lumen formation assay used 96-well plates coated with growth factor-reduced Matrigel (Corning, NY, USA). HUVECs (3×10^4 cells/well) were seeded in EGM-2 medium. After forming capillary-like structures, the medium was replaced with HepG2 or Huh7 cell supernatants. After 6 h, lumens were imaged with phase-contrast microscopy (OLYMPUS CKX53, Olympus, Japan) and quantified using Image J.

Statistical analysis

All statistical analyses were conducted using R (version 4.0.4). Differences between two groups were assessed with a two-tailed, unpaired Student's t-test. Chi-square tests examined correlations between LPRS and clinical features. Kaplan-Meier analyses for OS used the median LPRS, with significance by log-rank test. Univariate and multivariate Cox regression analyses identified relationships between variables and outcomes, with significance set at $P<0.05$.

Results

Variability in the genetic landscape of LLPS-related genes in HCC

In the TCGA-LIHC cohort analysis, we identified 652 DEGs (P-value and FDR < 0.05, and |log2FC| > 1). Among these, 519 genes were upregulated, and 133 genes were downregulated in HCC (Fig. 2A, B). These DEGs are

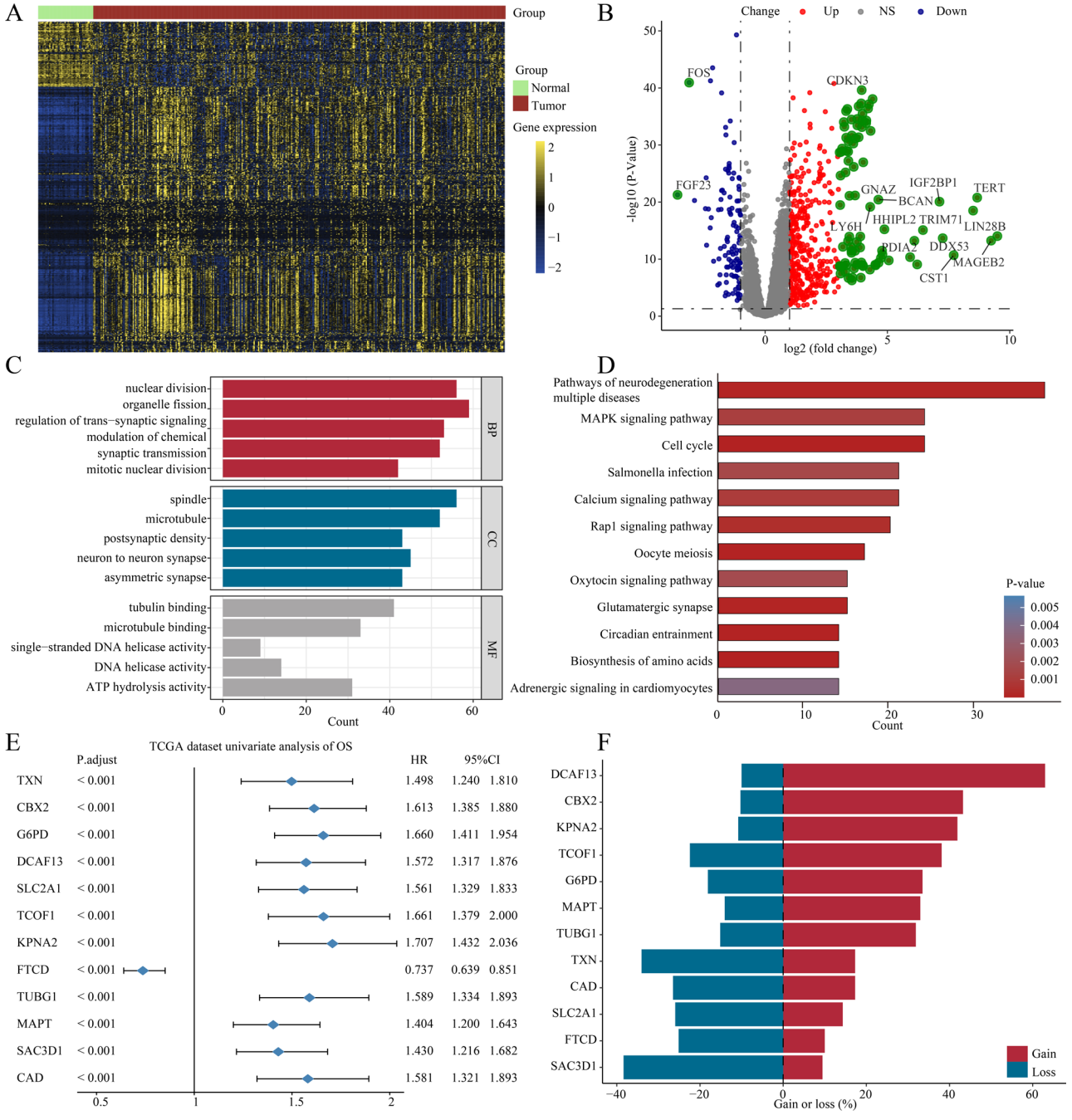

Fig. 2 The variation and prognostic value of LLPS in HCC. (**A**) Heatmap of the LLPS-related DEGs between HCC and normal tissues. (**B**) Volcano plot of the LLPS-related DEGs. (**C**) GO enrichment analyses based on the DEGs. (**D**) KEGG enrichment analyses based on the DEGs. (**E**) Univariate Cox analysis of OS in HCC. (**F**) CNV values of LLPS prognosis related genes in the TCGA cohort

detailed in Table S3. Functional enrichment analyses revealed that DEGs are involved in processes such as nuclear division, organelle fission, the cell cycle, and the MAPK signaling pathway (Fig. 2C, D). Univariate Cox analysis was initially conducted, identifying 330 DEGs closely associated with OS. Using bootstrapping, we identified 85 DEGs consistently correlated with prognosis. A minimal depth-based random survival forest (RSF) method selected the key features. After 1,000 RSF iterations, 12 genes with the highest C-index values were retained for further study. Figure 2E shows a forest plot representing the univariate Cox analysis of 12 genes in the TCGA-LIHC dataset. Additionally, CNV (copy number variation) status analysis showed frequent alterations in these 12 genes. It was noted that DCAF13 had the most CNV amplifications in pan-cancer and HCC,

whereas SLC2A1, FTCD, and SAC3D1 possessed the most significant copy number deletions in HCC (Fig. 2F and Fig. S1 A). The chromosomal locations of the 12 genes are shown in Fig. S1 B. The somatic mutation analysis indicated that the mutation rate of 12 genes in HCC patients was relatively low, at 4.35% (16/368) (Fig. S1 C). These results indicated that LLPS-related genes were dysregulated in HCC and had potential prognostic value.

Construction of LLPS-related prognostic risk score (LPRS) and its clinical value and pathway characteristic assessment

To determine the prognostic value of LLPS-related genes in HCC, we computed the LPRS incorporating TXN, CBX2, DCAF13, SLC2A1, KPNA2, FTCD, MAPT, and SAC3D1. The LPRS was derived using a LASSO Cox regression model based on the minimum criterion (Fig. 3A, B). The LPRS formula employed is as follows: LPRS = (0. 136× expression of TXN) + (0. 137× expression of CBX2) + (0. 080× expression of DCAF13) + (0. 114× expression of SLC2A1) + (0. 114× expression of KPNA2) + (-0.136 × expression of FTCD) + (0. 078× expression of MAPT) + (0. 164× expression of SAC3D1) in the training and validation cohorts. Stratifying HCC patients by median LPRS showed that high LPRS is significantly associated with reduced OS (Fig. 3C-E). In comparison with other LLPS-related models, the time-dependent AUC analysis revealed that the LPRS outperformed the Lai and Wang models in the training cohort (TCGA-LIHC) as well as in the two external validation cohorts (ICGC-LIRI and CHCC) (Fig. S2 A-C). Further analysis revealed that high LPRS was significantly correlated with high histologic grade (G3-G4), advanced TNM stage, vascular invasion, and poor five-year prognosis (Fig. 4A-E and Table S4). GSVA was used to identify differences in biological processes between high- and low-LPRS groups using data from the TCGA, ICGC, and CHCC datasets (Fig. 4F). This investigation revealed significant variations in eight distinct pathways across all datasets (Table S5). Subsequent validation via GSEA underscored a marked enrichment of pathways, including the unfolded protein response, MYC targets, E2F targets, G2M checkpoint, DNA repair, PI3K-AKT-MTOR signaling, and MTORC1 signaling, in samples exhibiting high LPRS levels, as determined by the TCGA-LIHC database (Fig. 4G-I and Fig. S3 A-C). Overall, LPRS shows promising clinical prognostic potential, likely associated with the regulation of the cell cycle and the PI3K-AKT pathway in HCC.

Creation and evaluation of the nomogram survival model

In subsequent analyses, both univariate and multivariate Cox regression analyses identified LPRS and TNM stage as independent prognostic factors in HCC (Fig. S3 D). Using the TCGA cohort, a nomogram model was developed through multivariate Cox and stepwise regression analyses to evaluate 1-, 3-, and 5-year OS, incorporating age, TNM stage, and LPRS as significant variables (Fig. 5A and Table S4). The model's accuracy was validated via calibration curves (Fig. 5B). Decision curve analysis (DCA) demonstrated that the nomogram model outperformed other clinical features (Fig. 5C). A significant divergence in survival between the high-LPRS and low-LPRS groups was evident based on the nomogram score (Fig. 5D). Additionally, the evaluation of AUC values for the public cohorts demonstrated the remarkable precision of the nomogram in forecasting 1-, 3-, and 5-year survival in HCC patients (Fig. 5E-G). In summary, our prognostic nomogram for OS prediction, based on these results, is considered reliable and suitable for implementation in HCC patient care.

Tumor microenvironment dissection based on LPRS

We further investigated the detailed distribution of the LPRS in HCC using scRNA data. By annotating the major cell types in GSE149614, we found that the LPRS in T/NK and hepatocyte cells differed from that in other cell types (Fig. 6A, B). The violin plot clearly demonstrated the variations in LPRS across cell types, consistently indicating higher LPRS in hepatocyte cells (Fig. 6C). Given the significant variation in LPRS within hepatocyte cells, we further annotated them into pro-metastatic, pro-tumorigenic, and non-malignant subgroups (Fig. 6D). We found that most pro-metastatic cells exhibited high LPRS, and pro-tumorigenic cells had significantly higher LPRS than non-malignant cells (Fig. 6E, F). Subsequently, the heatmap demonstrated that CBX2, SAC3D1, DCAF13, MAPT, and TXN were highly expressed in hepatocytes, particularly in pro-metastatic cells (Fig. 6G, H). These findings collectively suggest a close association between LPRS and the formation and metastasis of tumors.

Identification of potential therapeutic agents for high LPRS HCCs

To uncover potential drugs for treating high-LPRS HCC patients, our analysis began with an examination of CTRP and PRISM data. Initially, we conducted a differential drug response analysis comparing the top and bottom decile groups with the highest and lowest LPRS scores. Subsequently, analyzing the correlation of AUC values of drugs and LPRS was conducted, selecting drugs with a correlation coefficient less than −0.3. These analyses identified four CTRP-derived compounds (including Fluvastatin, Lovastatin, ABT-737, and MLN2238) and six PRISM-derived compounds (including KI-16425, Indiplon, Dofetilide, Dabrafenib, Puromycin, and LY2183240) (Fig. 7A, B). The results were further validated in HCC patients. The fold-change values, indicating increased

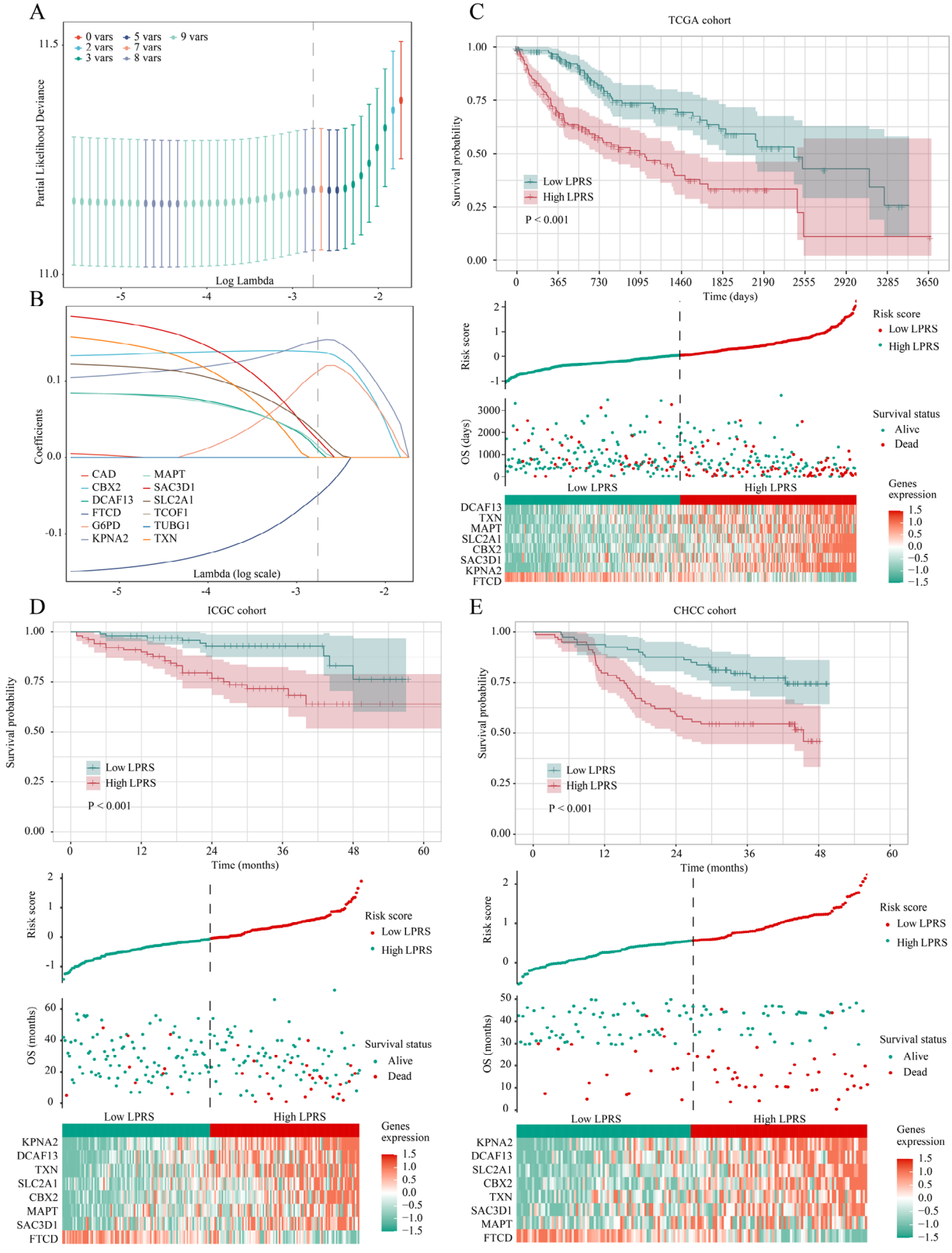

Fig. 3 Construction and validation of the LPRS signature. (**A**) Selection of the optimal parameter (lambda) in the LASSO model. (**B**). LASSO coefficients of the 12 LLPS-prognosis related genes in TCGA cohort. (**C**, **D** and **E**) Overall survival analysis for high-LPRS and low- LPRS groups in the training (TCGA) cohort and validation (ICGC, CHCC) cohort, respectively

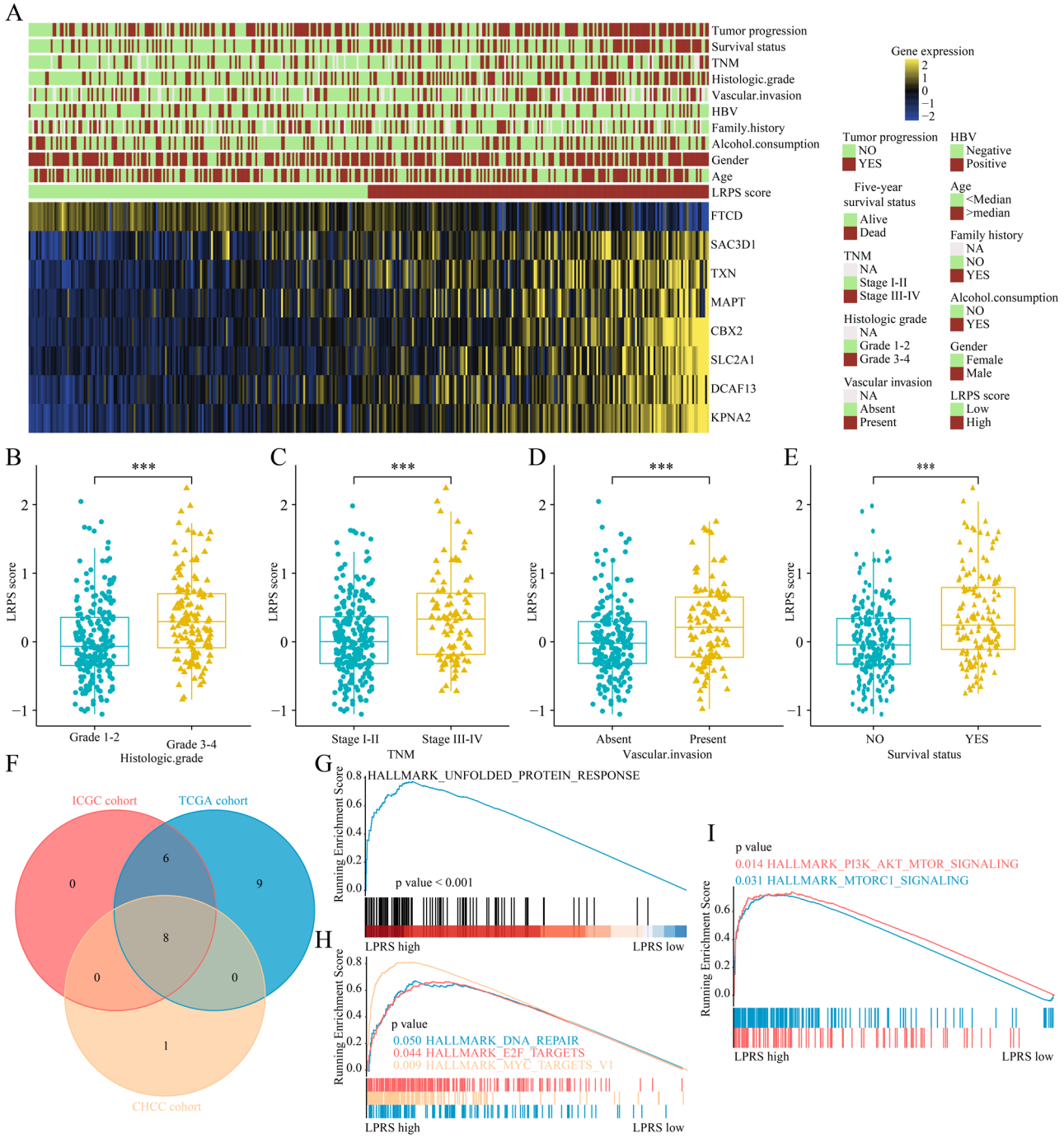

Fig. 4 LPRS Clinical Value and Pathway Characteristic Assessment. (**A**) Heatmap of eight LLPS prognosis related genes expression and corresponding clinicopathological features of low- and high- LPRS group. (**B**-**E**) The relationships between the LPRS and clinical characteristics including histologic grade, TNM stage, vascular invasion and survival status. (**F**) Venn diagram derived from Gene Set Variation Analysis (GSVA). (**G**-**I**) Gene Set Enrichment Analysis (GSEA) enrichment results based on the TCGA database

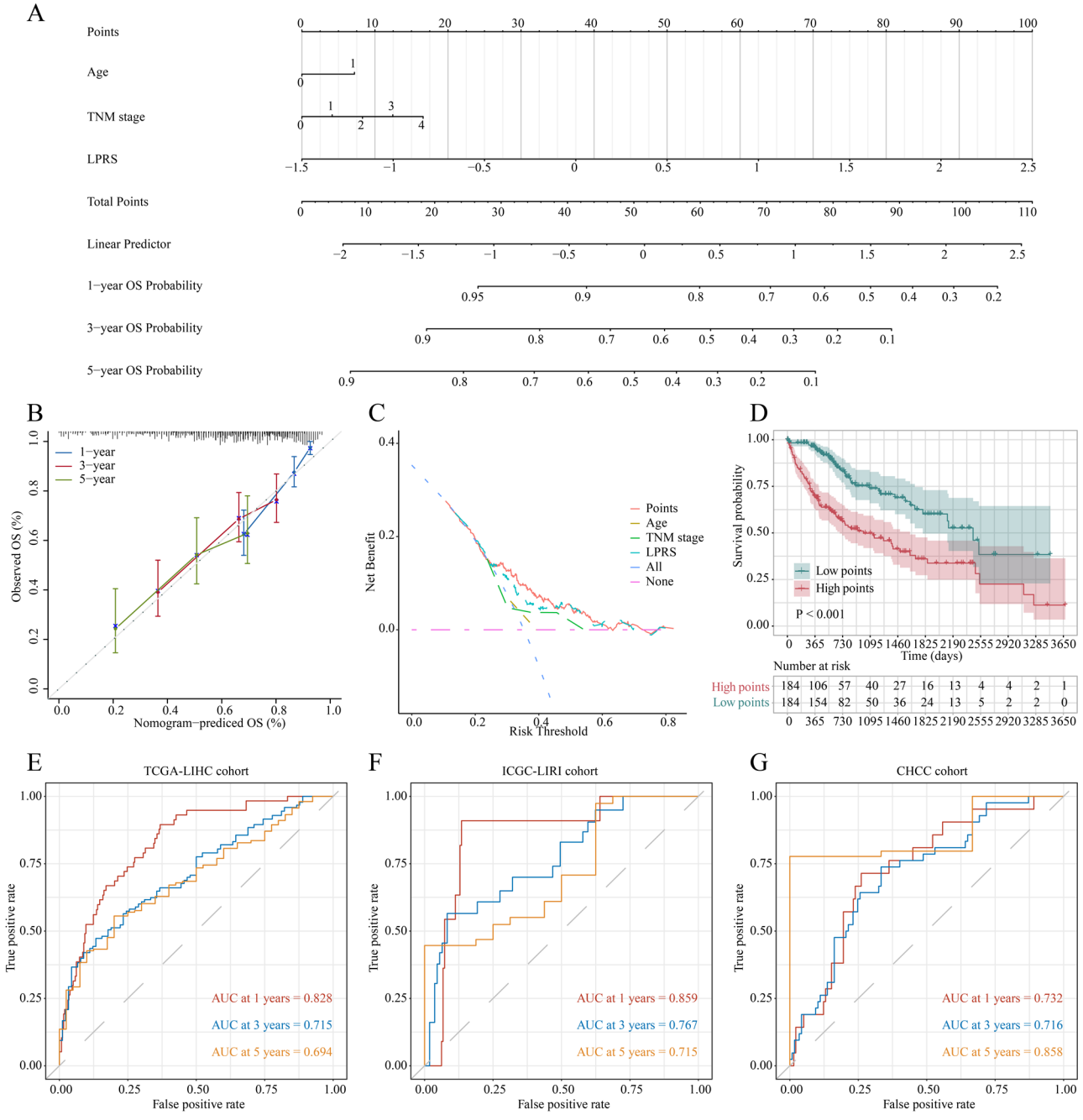

Fig. 5 Establishment and assessment of the nomogram survival model. (**A**) A nomogram was established to predict the prognostic of HCC patients. (**B**) Calibration plots showing the probability of 1-, 3-, and 5-year overall survival in TCGA cohort. (**C**) Decision curve analysis (DCA) of nomogram predicting overall survival. (**D**) Kaplan-Meier analyses for the two HCC groups based on the nomogram score. (**E**-**G**) Receiver operator characteristic (ROC) analysis of nomogram predicting 1-, 3-, and 5-year overall survival in TCGA-LIHC, ICGC-LIRI and CHCC cohort

expression of drug target genes in tumor tissue compared to normal tissue, suggest these drug candidates are more likely to treat HCC effectively. Additionally, an extensive search of the PubMed database and https://www.clinicaltrials.gov/ was conducted to find studies and clinical trials supporting the efficacy of these drug candidates (Fig. 7C). Navitoclax shows promising results for treating high-LPRS score HCC, owing to its outstanding in silico and in vitro performance.

Model interpretation and important molecular screening based on SurvSHAP

SurvSHAP, the pioneering method in providing time-dependent explanations for survival regression DL models, represents a significant advancement in the field. In

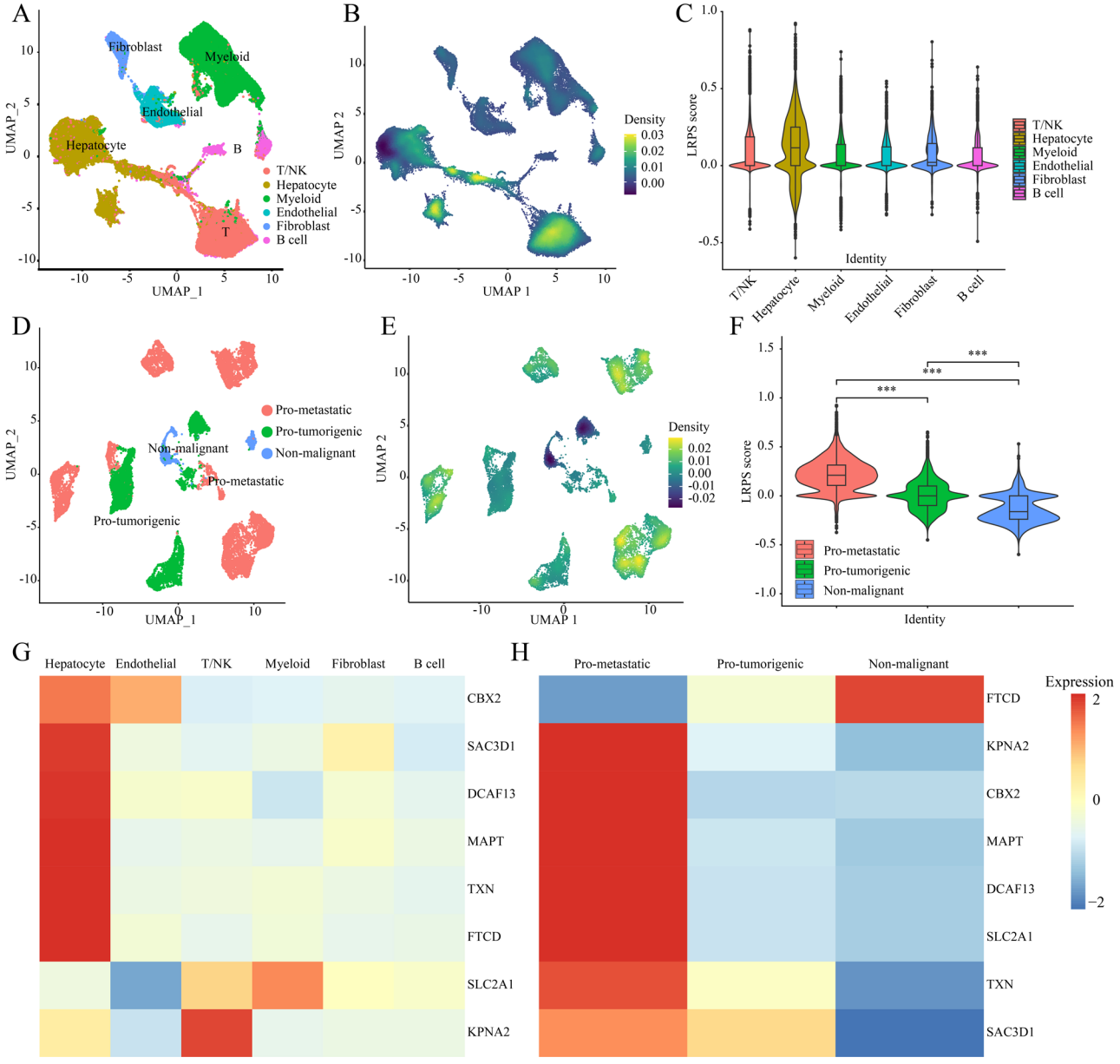

Fig. 6 Analysis of the Tumor Microenvironment Utilizing the LPRS Signature. (**A**) UMAP plot visualization of cell subtypes across 21 HCC patients. (**B**) UMAP plot depicting the density of LPRS. (**C**) Violin plots representing the LPRS value across different cell types. (**D**) UMAP plot illustrating the annotations of hepatocyte cells in an HCC patient. (**E**) UMAP plot showing the density of LPRS in hepatocyte subgroups. (**F**) Violin plots of LPRS values in various hepatocyte subgroups. (**G**-**H**) Heatmaps displaying the distribution of genes from the 8-gene LPRS model within the cellular subtypes of the HCC microenvironment

Fig. 8A and B, we depict the aggregation of the seven most crucial variables, sorted by their aggregated Shapley values, across 500 observations. The horizontal bars illustrate the frequency of observations where a variable's importance, indicated by a specific color, ranked first, second, and so on. Significantly, CBX2 emerged as the paramount variable, with subsequent importance attributed to DCAF13 and SAC3D1.

DCAF13 is a key player in the LPRS and a tumor promoter in HCC

After a comprehensive analysis of all findings, we identified DCAF13 as the key gene linked to the LPRS signature, conducting further experiments. Employing qRT-PCR experiments, we quantified the mRNA levels of DCAF13 in HCC and adjacent tissue samples from the HX-cohort. Differential analysis disclosed a notable increase in DCAF13 expression in HCC tissue samples (Fig. 9A). Further analysis of clinical characteristics

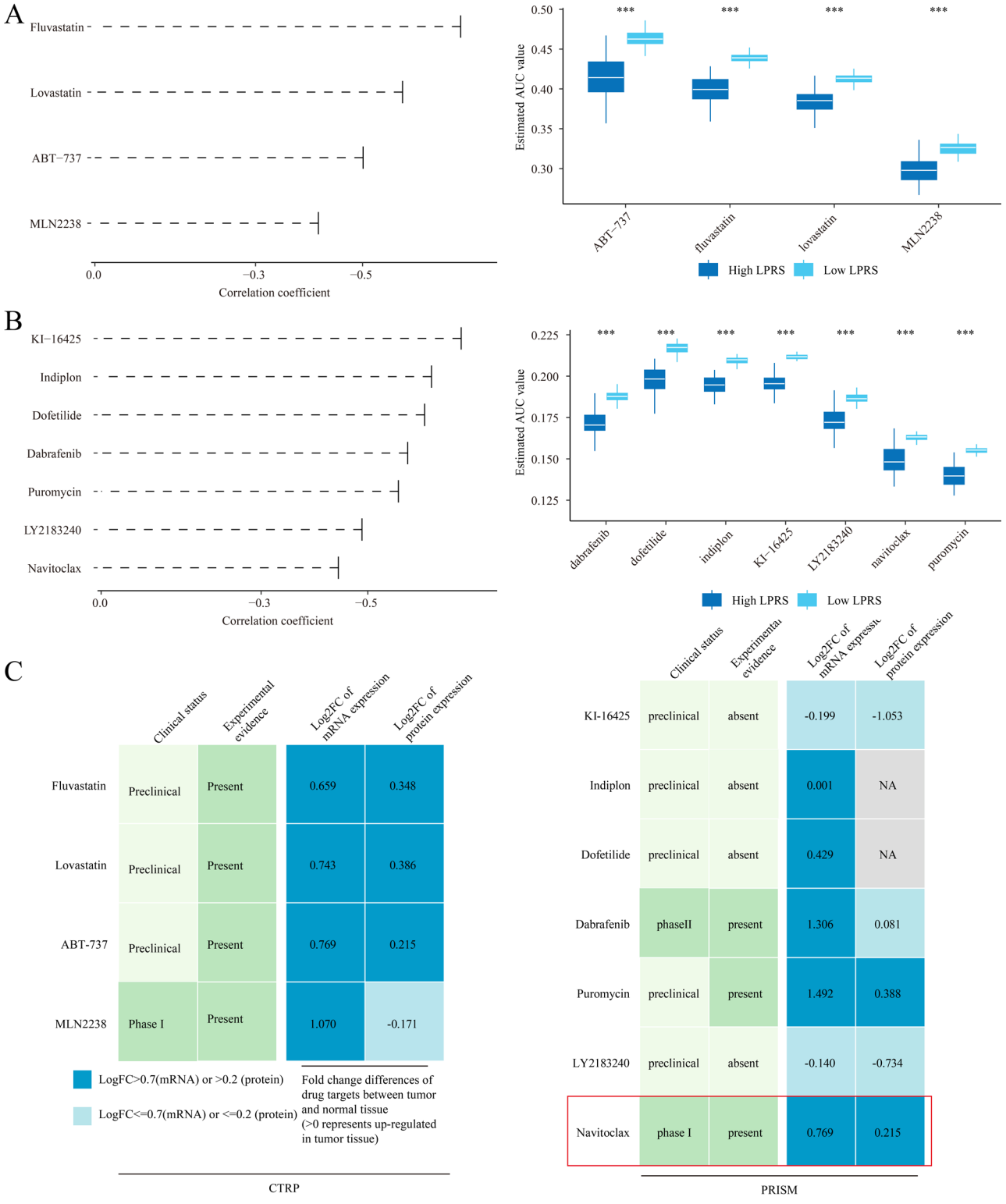

Fig. 7 Identifying Potential Therapeutics with Enhanced Sensitivity in High LPRS Patients. (**A**) Spearman's correlation and differential response analysis for four CTRP-derived compounds, with lower y-axis values indicating higher drug sensitivity. (**B**) Analysis of seven PRISM-derived compounds using Spearman's correlation and differential response, where lower y-axis values denote increased sensitivity. (**C**) Pinpointing the most effective therapeutic agents for high LPRS patients, supported by multi-source evidence

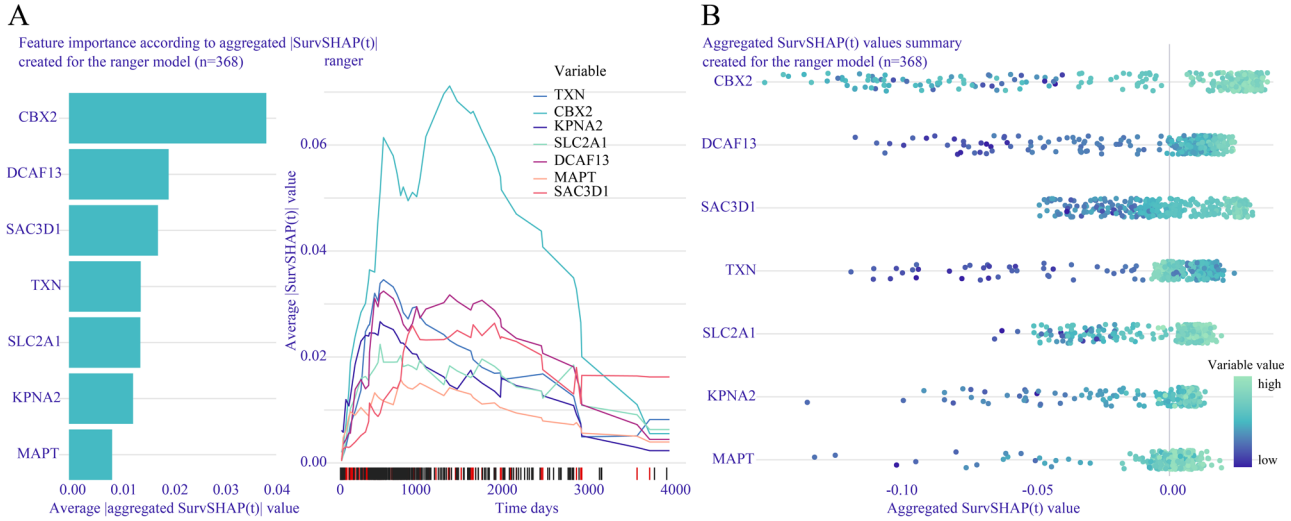

Fig. 8 Model interpretation based on SurvSHAP. (**A**) Time dependent SurvSHAP(t) value. (**B**) The rank of eight LPRS related genes according to the SHAP value

revealed markedly higher expression of DCAF13 in BCLC stage (stage C and D) tissues, with survival analysis indicating a strong correlation between elevated DCAF13 expression and an unfavorable prognosis in HCC patients (Fig. 9B; Table S6). Subsequently, we conducted in vitro cell experiments. Through siRNA-mediated knockdown, DCAF13 protein levels were diminished in Huh7 and HepG2 cells. Additionally, we assessed the protein levels of HCC progression markers in siRNA-transfected cells to validate whether DCAF13 alteration induced changes in HCC progression marker genes. As expected, DCAF13 silencing suppressed the protein expression of HIF-1α, VEGF, NOTCH-1, β-catenin, c-Myc, and CCND1 (Fig. 9C). Both the CCK8 cell proliferation assays and clonal experiments demonstrated significant growth inhibition in both Huh7 and HepG2 cell lines with DCAF13 reduction (Fig. 9D and E). Subsequent evaluation of the effects of DCAF13 silencing on tube formation in Huh7 and HepG2 cells revealed a significant inhibitory effect on HCC cell tube junctions and length (Fig. 9F). Up to this point, our data substantiates the pivotal role of DCAF13 in the proliferation and metastasis of HCC.

Discussion

Recent advancements in LLPS have significantly impacted our comprehension of how tumors develop malignant characteristics [35–37]. Therefore, we embarked on investigating the clinical relevance and molecular mechanisms of LLPS-related genes in HCC. Within this study, LLPS genes exhibiting varied expression patterns and prognostic significance in HCC were identified as potential prognostic biomarkers for the disease. These genes include CBX2, DCAF13, SAC3D1, TXN, SLC2A1, KPNA2, MAPT, and FTCD. Their respective roles in the LLPS process are meticulously delineated in Table S7.

Previous studies have demonstrated that CBX2 promotes the phase separation of DNA and nucleosomes, leading to the formation of condensates that regulate chromatin compaction, modulate downstream gene expression, and ultimately influence tumor function [38]. In HCC, CBX2 has been identified as an oncogene. Silencing CBX2 has been shown to enhance YAP phosphorylation, which in turn suppresses HCC cell proliferation and promotes apoptosis [39]. This is consistent with our research, where CBX2 ranks highest in SHAP values for the prognosis of HCC. Subsequently, SAC3D1 was found to be associated with centrosome replication and spindle formation during the cell cycle [40]. Furthermore, SAC3D1 has been identified as a potential prognostic biomarker for HCC Moreover, single-cell data indicate specific high expression of SAC3D1 in HCC stem cells [41, 42]. However, there is still a lack of relevant in vitro and in vivo experiments. TXN regulates the formation of stress granules through phase separation, thereby affecting the proliferation and apoptosis of tumor cells [43]. In addition, in vitro and in vivo experiments have confirmed that TXN promotes hepatocarcinogenesis, proliferation, and metastasis of HCC [44]. Its mechanism is associated with increased stability of BACH1 and activation of the AKT/mTOR pathway [45]. SLC2A1 has been shown to be associated with the formation of the postsynaptic density [46]. SLC2A1 has been proven to be a promoter molecule of HCC, associated with the metastasis, drug resistance, and immune escape of HCC. Its mechanism is related to the Warburg effect of tumors, making it a potential therapeutic target for HCC [47]. KPNA2 is a nuclear transport protein responsible for transporting proteins from the cytoplasm to the cell nucleus, and it is associated

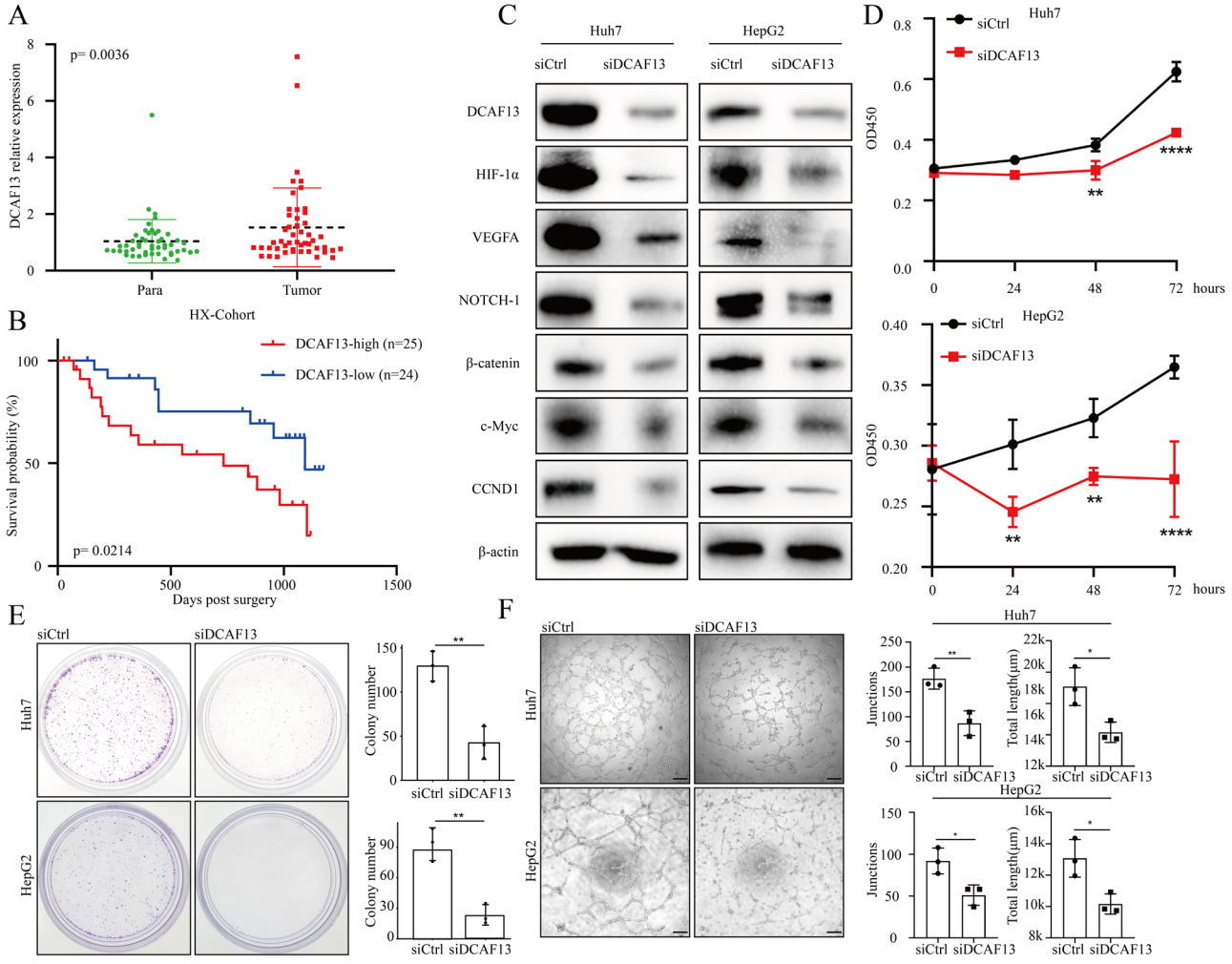

Fig. 9 Clinical significance, prognostic value, and biological function of DCAF13 in HCC. (**A**) The mRNA levels of the DCAF13 were determined in HCC tissues and adjacent normal samples. (**B**) Kaplan–Meier survival curves according to DCAF13 expression in HCC specimens. (**C**) Western blot analysis of HIF-1α, VEGF, NOTCH-1, β-catenin, c-Myc, and CCND1 in Huh7 and HepG2 cells. (**D**) CCK-8 assay was used to evaluate the cell proliferation of Huh7 and HepG2 cells. (**E**) Colony formation assay was used to evaluate the cell proliferation of Huh7 and HepG2 cells. (**F**) Representative pictures of lumen formation assay

with the formation of structures such as the nucleolus [48]. In HCC, KPNA2 plays a pivotal role in promoting tumor proliferation and migration by regulating DNA replication and the cell cycle [49]. Meanwhile, microtubule-associated protein tau (MAPT) has been identified to undergo LLPS through homotypic interaction via self-coacervation or heterotypic association through complex-coacervation with binding partners such as RNA [50]. MAPT has been implicated as an oncogene in various cancers, including breast cancer, gastric cancer, prostate cancer, and brain cancer. In the context of HCC, the overexpression of MAPT significantly enhances the proliferation and migration capabilities of HCC cells [51]. Furthermore, FTCD is involved in the formation of the centrosome. In HCC, there is a notable downregulation in the expression of FTCD. This loss of FTCD expression leads to the upregulation of PPAR-γ and SREBP2 by modulating the PTEN/Akt/mTOR signaling axis [52]. Consequently, this dysregulation results in lipid accumulation and contributes to hepatocarcinogenesis. DCAF13 function as a component of the E3 ubiquitin ligase complex, participating in various biological processes such as cell cycle regulation, DNA repair, and immune response [53]. These intricate roles underscore the multifaceted nature of DCAF13 in cellular homeostasis and disease pathogenesis, including its potential involvement in hepatocellular carcinoma progression. The phase separation of NPM1/DCAF13 plays a crucial regulatory role in ribosome maturation [54]. The dysregulation of DCAF13 expression in HCC is prognostically relevant and clinically significant. While the oncogenic role of DCAF13 has been confirmed in breast cancer and lung adenocarcinoma, its role in HCC is yet to be explored [55–57]. Further investigation revealed that elevated DCAF13 expression is associated with adverse clinical outcomes and BCLA grading (C-D), and in vitro experiments

confirmed that decreased DCAF13 expression inhibits the proliferation and angiogenesis of HCC cells. Therefore, DCAF13 may play a crucial role in HCC through LLPS, but further molecular mechanisms require in-depth exploration.

Based on the eight potential LLPS prognosis-related genes, we formulated the LPRS and explored its prognostic and predictive significance, alongside its robust correlations with HCC. Our findings reveal a distinct segregation in survival trends between cohorts exhibiting high versus low LPRS levels. Notably, our investigation indicates that individuals with high LPRS exhibit inferior clinical status and survival outcomes compared to those harboring lower LPRS levels. Moreover, we identified significant enrichment of genes related to the unfolded protein response, cell cycle, and PI3K-AKT-MTOR pathways in high-LPRS samples through GSVA and GSEA analyses. Previous studies have linked unfolded protein accumulation in the endoplasmic reticulum (ER) lumen to HCC progression, metastasis, and drug resistance [58, 59]. Furthermore, the crosstalk between the unfolded protein response and the PI3K/AKT/mTOR pathway is critical in shaping cancer cell fate [60]. Therefore, LLPS may drive hepatocellular carcinoma progression through the interplay of the unfolded protein response, PI3K/AKT signaling, and cell cycle-related pathways. Subsequently, we devised a prognostic nomogram by amalgamating LPRS, TNM stage, and age, which demonstrated commendable performance in prognosticating and enhancing the precision of survival estimations.

The related research shows that alterations in phase separation form the basis of many cancer phenotypes. Mutations in a few genes can alter the ability of macromolecules to form biomolecular condensates, indirectly affecting their activity. This provides a non-genetic explanation for tumor heterogeneity and drug resistance. Therefore, in this study, we evaluated the impact of LPRS on the HCC microenvironment based on single-cell sequencing data. It is noteworthy that in HCC, LLPS may primarily affect the metastasis of HCC cells through CBX2, SAC3D1, DCAF13, MAPT, and TXN, thereby influencing the prognosis of HCC. Systematic drug screening revealed that navitoclax is a potential therapeutic drug for patients with high-LPRS HCC patients. Its mechanism of action involves targeting and inhibiting specific Bcl-2 family proteins to promote apoptosis of cancer cells, thereby inhibiting tumor growth [61]. Due to the poor solubility and low bioavailability of ABT-737, a clinical formulation of ABT-737, navitoclax, has been developed. Preliminary in vitro and in vivo experiments have confirmed the therapeutic effect of navitoclax on HCC, and related clinical trials are underway [62]. However, this research primarily relies on bioinformatics analyses, which, while robust, necessitate further validation in multicenter clinical cohorts to comprehensively evaluate the prognostic value of the LPRS model in HCC. Additionally, the molecular mechanism by which DCAF13 participates in HCC progression through LLPS remains to be fully elucidated. The association between LLPS and navitoclax sensitivity in HCC also requires further mechanistic exploration.

Conclusions

Essentially, we devised an innovative LPRS model capable of accurately forecasting the clinical prognosis and drug sensitivity of HCC. LLPS potentially influences the prognosis of HCC by modulating its metastatic behavior. Furthermore, there is suggestive evidence implicating DCAF13 as a key player in the LLPS-mediated malignant progression of HCC.

Supplementary Information

The online version contains supplementary material available at https://doi.org/10.1186/s13062-025-00592-4.

Supplementary Material 1

Supplementary Material 2

Supplementary Material 3

Acknowledgements

We express our gratitude to Shipeng Guo and all members of the GZDlab for their participation in the discussion of this study with the first author, as well as their invaluable help and support.

Author contributions

JH L performed all the experimental work. H T and L B conceived and participated in the design of the study. The manuscript was written by Jh Li and H C. All authors read and approved the final manuscript.

Funding

This work was supported by the National Key Research and Development Program of China (NO.2022YFC2304800), National Natural Science Foundation of China (82172254) and 1.3.5 project for disciplines of excellence, West China Hospital, Sichuan University (No. ZYGD23030).

Data availability

No datasets were generated or analysed during the current study.

Declarations

Ethics approval and consent to participate

The study was authorized by the West China Hospital's Medical Ethics Committee (Number 91 of the year 2016) and conducted in accordance with the Declaration of Helsinki. Written informed consent was collected according to the ethical regulations of West China Hospital.

Consent for publication

Not applicable.

Competing interests

The authors declare no competing interests.

Received: 1 July 2024 / Accepted: 2 January 2025
Published online: 06 January 2025

References

1. Kole C, Charalampakis N, Tsakatikas S, Vailas M, Moris D, Gkotsis E, Kykalos S, Karamouzis MV, Schizas D. Immunotherapy for Hepatocellular Carcinoma: a 2021 Update. Cancers 2020, 12(10).
2. Foerster F, Gairing SJ, Ilyas SI, Galle PR. Emerging immunotherapy for HCC: a guide for hepatologists. Hepatology (Baltimore MD). 2022;75(6):1604–26.
3. Llovet JM, Kelley RK, Villanueva A, Singal AG, Pikarsky E, Roayaie S, Lencioni R, Koike K, Zucman-Rossi J, Finn RS. Hepatocellular carcinoma. Nat Reviews Disease Primers. 2021;7(1):6.
4. Sperandio RC, Pestana RC, Miyamura BV, Kaseb AO. Hepatocellular Carcinoma Immunotherapy. Annu Rev Med. 2022;73:267–78.
5. Tang W, Chen Z, Zhang W, Cheng Y, Zhang B, Wu F, Wang Q, Wang S, Rong D, Reiter FP, et al. The mechanisms of sorafenib resistance in hepatocellular carcinoma: theoretical basis and therapeutic aspects. Signal Transduct Target Therapy. 2020;5(1):87.
6. Dai X, Guo Y, Hu Y, Bao X, Zhu X, Fu Q, Zhang H, Tong Z, Liu L, Zheng Y, et al. Immunotherapy for targeting cancer stem cells in hepatocellular carcinoma. Theranostics. 2021;11(7):3489–501.
7. Wang Z, Wang Y, Gao P, Ding J. Immune checkpoint inhibitor resistance in hepatocellular carcinoma. Cancer Lett. 2023;555:216038.
8. Moldogazieva NT, Zavadskiy SP, Sologova SS, Mokhosoev IM, Terentiev AA. Predictive biomarkers for systemic therapy of hepatocellular carcinoma. Expert Rev Mol Diagn. 2021;21(11):1147–64.
9. Oldenhuis CN, Oosting SF, Gietema JA, de Vries EG. Prognostic versus predictive value of biomarkers in oncology. Eur J cancer (Oxford England: 1990). 2008;44(7):946–53.
10. Yu B, Ma W. Biomarker discovery in hepatocellular carcinoma (HCC) for personalized treatment and enhanced prognosis. Cytokine Growth Factor Rev. 2024;79:29–38.
11. Wu T, Luo G, Lian Q, Sui C, Tang J, Zhu Y, Zheng B, Li Z, Zhang Y, Zhang Y, et al. Discovery of a carbamoyl phosphate synthetase 1-Deficient HCC Subtype with therapeutic potential through integrative genomic and experimental analysis. Hepatology (Baltimore MD). 2021;74(6):3249–68.
12. Li J, Wang W, Zhou Y, Liu L, Zhang G, Guan K, Cui X, Liu X, Huang M, Cui G, et al. m6A Regulator-Associated modification patterns and Immune Infiltration of the Tumor Microenvironment in Hepatocarcinoma. Front cell Dev Biology. 2021;9:687756.
13. Wang C, Yang G, Feng G, Deng C, Zhang Q, Chen S. Developing an advanced diagnostic model for hepatocellular carcinoma through multi-omics integration leveraging diverse cell-death patterns. Front Immunol. 2024;15:1410603.
14. Alberti S, Gladfelter A, Mittag T. Considerations and challenges in studying liquid-liquid phase separation and Biomolecular condensates. Cell. 2019;176(3):419–34.
15. Bracha D, Walls MT, Brangwynne CP. Probing and engineering liquid-phase organelles. Nat Biotechnol. 2019;37(12):1435–45.
16. Alberti S, Hyman AA. Biomolecular condensates at the nexus of cellular stress, protein aggregation disease and ageing. Nat Rev Mol Cell Biol. 2021;22(3):196–213.
17. Wiedner HJ, Giudice J. It's not just a phase: function and characteristics of RNA-binding proteins in phase separation. Nat Struct Mol Biol. 2021;28(6):465–73.
18. Wagh K, Garcia DA, Upadhyaya A. Phase separation in transcription factor dynamics and chromatin organization. Curr Opin Struct Biol. 2021;71:148–55.
19. Cheng Y, Xie W, Pickering BF, Chu KL, Savino AM, Yang X, Luo H, Nguyen DT, Mo S, Barin E, et al. N(6)-Methyladenosine on mRNA facilitates a phase-separated nuclear body that suppresses myeloid leukemic differentiation. Cancer Cell. 2021;39(7):958–e972958.
20. Pakravan D, Orlando G, Bercier V, Van Den Bosch L. Role and therapeutic potential of liquid-liquid phase separation in amyotrophic lateral sclerosis. J Mol Cell Biol. 2021;13(1):15–28.
21. Kanekura K, Kuroda M. How can we interpret the relationship between liquid-liquid phase separation and amyotrophic lateral sclerosis? Lab Invest. 2022;102(9):912–8.
22. Ainani H, Bouchmaa N, Ben Mrid R, El Fatimy R. Liquid-liquid phase separation of protein tau: an emerging process in Alzheimer's disease pathogenesis. Neurobiol Dis. 2023;178:106011.
23. Boyko S, Surewicz WK. Tau liquid-liquid phase separation in neurodegenerative diseases. Trends Cell Biol. 2022;32(7):611–23.
24. Fu Q, Zhang B, Chen X, Chu L. Liquid-liquid phase separation in Alzheimer's disease. J Mol Med. 2024;102(2):167–81.
25. Liu Q, Li J, Zhang W, Xiao C, Zhang S, Nian C, Li J, Su D, Chen L, Zhao Q, et al. Glycogen accumulation and phase separation drives liver tumor initiation. Cell. 2021;184(22):5559–e55765519.
26. Cai D, Feliciano D, Dong P, Flores E, Gruebele M, Porat-Shliom N, Sukenik S, Liu Z, Lippincott-Schwartz J. Phase separation of YAP reorganizes genome topology for long-term YAP target gene expression. Nat Cell Biol. 2019;21(12):1578–89.
27. Cloer EW, Siesser PF, Cousins EM, Goldfarb D, Mowrey DD, Harrison JS, Weir SJ, Dokholyan NV, Major MB. p62-Dependent phase separation of patient-derived KEAP1 mutations and NRF2. Mol Cell Biol 2018, 38(22).
28. Lu Y, Yang A, Quan C, Pan Y, Zhang H, Li Y, Gao C, Lu H, Wang X, Cao P, et al. A single-cell atlas of the multicellular ecosystem of primary and metastatic hepatocellular carcinoma. Nat Commun. 2022;13(1):4594.
29. Ning W, Guo Y, Lin S, Mei B, Wu Y, Jiang P, Tan X, Zhang W, Chen G, Peng D, et al. DrLLPS: a data resource of liquid-liquid phase separation in eukaryotes. Nucleic Acids Res. 2020;48(D1):D288–95.
30. Wu T, Hu E, Xu S, Chen M, Guo P, Dai Z, Feng T, Zhou L, Tang W, Zhan L, et al. clusterProfiler 4.0: a universal enrichment tool for interpreting omics data. Innov (Cambridge (Mass). 2021;2(3):100141.
31. Ghandi M, Huang FW, Jané-Valbuena J, Kryukov GV, Lo CC, McDonald ER 3rd, Barretina J, Gelfand ET, Bielski CM, Li H, et al. Next-generation characterization of the Cancer Cell Line Encyclopedia. Nature. 2019;569(7757):503–8.
32. Yang C, Huang X, Li Y, Chen J, Lv Y, Dai S. Prognosis and personalized treatment prediction in TP53-mutant hepatocellular carcinoma: an in silico strategy towards precision oncology. Brief Bioinform 2021, 22(3).
33. Zhu E, Zhang L, Wang J, Hu C, Pan H, Shi W, Xu Z, Ai P, Shan D, Ai Z. Deep learning-guided adjuvant chemotherapy selection for elderly patients with breast cancer. *Breast cancer research and treatment* 2024.
34. Data from Warsaw University of Technology Provide New Insights into Machine Learning [Survshap(T). Time-dependent Explanations of Machine Learning Survival Models] %J Robotics & Machine Learning Daily News. 2023.
35. Zhang H, Ji X, Li P, Liu C, Lou J, Wang Z, Wen W, Xiao Y, Zhang M, Zhu X. Liquid-liquid phase separation in biology: mechanisms, physiological functions and human diseases. Sci China Life Sci. 2020;63(7):953–85.
36. Tong X, Tang R, Xu J, Wang W, Zhao Y, Yu X, Shi S. Liquid-liquid phase separation in tumor biology. Signal Transduct Target Therapy. 2022;7(1):221.
37. Yan X, Zhang M, Wang D. Interplay between posttranslational modifications and liquid–liquid phase separation in tumors. Cancer Lett. 2024;584:216614.
38. Akiba K, Katoh-Fukui Y, Yoshida K, Narumi S, Miyado M, Hasegawa Y, Fukami M. Role of liquid-liquid separation in endocrine and living cells. J Endocr Soc. 2021;5(10):bvab126.
39. Mao J, Tian Y, Wang C, Jiang K, Li R, Yao Y, Zhang R, Sun D, Liang R, Gao Z, et al. CBX2 regulates proliferation and apoptosis via the phosphorylation of YAP in Hepatocellular Carcinoma. J Cancer. 2019;10(12):2706–19.
40. Khuda SE, Yoshida M, Xing Y, Shimasaki T, Takeya M, Kuwahara K, Sakaguchi N. The Sac3 homologue shd1 is involved in mitotic progression in mammalian cells. J Biol Chem. 2004;279(44):46182–90.
41. Liu Y, He M, Ke X, Chen Y, Zhu J, Tan Z, Chen J. Centrosome amplification-related signature correlated with immune microenvironment and treatment response predicts prognosis and improves diagnosis of hepatocellular carcinoma by integrating machine learning and single-cell analyses. Hep Intl. 2024;18(1):108–30.
42. Han ME, Kim JY, Kim GH, Park SY, Kim YH, Oh SO. SAC3D1: a novel prognostic marker in hepatocellular carcinoma. Sci Rep. 2018;8(1):15608.
43. Jain S, Wheeler JR, Walters RW, Agrawal A, Barsic A, Parker R. ATPase-Modulated stress granules contain a diverse proteome and substructure. Cell. 2016;164(3):487–98.
44. Lei H, Wang G, Zhang J, Han Q. Inhibiting TrxR suppresses liver cancer by inducing apoptosis and eliciting potent antitumor immunity. Oncol Rep. 2018;40(6):3447–57.
45. Wang C, Zhang L, Cao M, Fu Z, Wang H, Zhang S, Zhu K, Hou Z, Cui J, Yue P, et al. Thioredoxin facilitates hepatocellular carcinoma stemness and metastasis by increasing BACH1 stability to activate the AKT/mTOR pathway. FASEB Journal: Official Publication Federation Am Soc Experimental Biology. 2023;37(6):e22943.
46. Bayés A, Collins MO, Croning MD, van de Lagemaat LN, Choudhary JS, Grant SG. Comparative study of human and mouse postsynaptic proteomes finds high compositional conservation and abundance differences for key synaptic proteins. PLoS ONE. 2012;7(10):e46683.
47. Amann T, Hellerbrand C. GLUT1 as a therapeutic target in hepatocellular carcinoma. Expert Opin Ther Targets. 2009;13(12):1411–27.

48. Yoshizawa T, Ali R, Jiou J, Fung HYJ, Burke KA, Kim SJ, Lin Y, Peeples WB, Saltzberg D, Soniat M, et al. Nuclear import receptor inhibits phase separation of FUS through binding to multiple sites. Cell. 2018;173(3):693–e705622.
49. Chen T, Liu R, Niu Y, Mo H, Wang H, Lu Y, Wang L, Sun L, Wang Y, Tu K, et al. HIF-1α-activated long non-coding RNA KDM4A-AS1 promotes hepatocellular carcinoma progression via the miR-411-5p/KPNA2/AKT pathway. Cell Death Dis. 2021;12(12):1152.
50. Ambadipudi S, Biernat J, Riedel D, Mandelkow E, Zweckstetter M. Liquid-liquid phase separation of the microtubule-binding repeats of the Alzheimer-related protein tau. Nat Commun. 2017;8(1):275.
51. Wang B, Nie CH, Xu J, Wan DL, Xu X, He JJ. Bigelovin inhibits hepatocellular carcinoma cell growth and metastasis by regulating the MAPT-mediated Fas/FasL pathway. Neoplasma. 2023;70(2):208–15.
52. Wang S, Zhou Y, Yu R, Ling J, Li B, Yang C, Cheng Z, Qian R, Lin Z, Yu C, et al. Loss of hepatic FTCD promotes lipid accumulation and hepatocarcinogenesis by upregulating PPARγ and SREBP2. JHEP Reports: Innov Hepatol. 2023;5(10):100843.
53. Boisvert FM, Lam YW, Lamont D, Lamond AI. A quantitative proteomics analysis of subcellular proteome localization and changes induced by DNA damage. Mol Cell Proteomics: MCP. 2010;9(3):457–70.
54. Zhou L, Wang S, Hu W, Liu X, Xu L, Tong B, Zhang T, Xue Z, Guo Y, Zhao J et al. T cell proliferation requires ribosomal maturation in nucleolar condensates dependent on DCAF13. J Cell Biol 2023, 222(10).
55. Wei S, Xing J, Chen J, Chen L, Lv J, Chen X, Li T, Yu T, Wang H, Wang K, et al. DCAF13 inhibits the p53 signaling pathway by promoting p53 ubiquitination modification in lung adenocarcinoma. J Experimental Clin cancer Research: CR. 2024;43(1):3.
56. Shan BQ, Wang XM, Zheng L, Han Y, Gao J, Lv MD, Zhang Y, Liu YX, Zhang H, Chen HS, et al. DCAF13 promotes breast cancer cell proliferation by ubiquitin inhibiting PERP expression. Cancer Sci. 2022;113(5):1587–600.
57. Sun Z, Zhou D, Yang J, Zhang D. Doxorubicin promotes breast cancer cell migration and invasion via DCAF13. FEBS open bio. 2022;12(1):221–30.
58. Pavlović N, Heindryckx F. Targeting ER stress in the hepatic tumor microenvironment. FEBS J. 2022;289(22):7163–76.
59. Dai R, Chen R, Li H. Cross-talk between PI3K/Akt and MEK/ERK pathways mediates endoplasmic reticulum stress-induced cell cycle progression and cell death in human hepatocellular carcinoma cells. Int J Oncol. 2009;34(6):1749–57.
60. Mafi S, Ahmadi E, Meehan E, Chiari C, Mansoori B, Sadeghi H, Milani S, Jafarinia M, Taeb S, Mafakheri Bashmagh B, et al. The mTOR Signaling Pathway interacts with the ER stress response and the unfolded protein response in Cancer. Cancer Res. 2023;83(15):2450–60.
61. Mohamad Anuar NN, Nor Hisam NS, Liew SL, Ugusman A. Clinical review: Navitoclax as a pro-apoptotic and anti-fibrotic Agent. Front Pharmacol. 2020;11:564108.
62. Yalniz FF, Wierda WG. Targeting BCL2 in chronic lymphocytic leukemia and other hematologic malignancies. Drugs. 2019;79(12):1287–304.

Publisher's note